A Novel Synchronously Rotating Reference Frame Based Adaptive Control Architecture for Enhanced Grid Support Functions of Single-Phase Inverters

Robin Bisht, *Student Member, IEEE*, Rojan Bhattarai, *Member, IEEE*, Shashank Subramaniam, *Member, IEEE*, and Sukumar Kamalasadan, *Senior Member, IEEE*

***Abstract*—This article presents a novel adaptive control architecture for—connected single-phase inverters (SPIs) that can dynamically regulate active and reactive power, thus enabling grid support functions effectively. The base controller framework is that of the active and reactive power control in the *dq*-domain. The proposed controller is based on an adaptive minimum variance framework and utilizes an online parametric identifier. The advantage of the proposed scheme is that the architecture can concurrently provide voltage support and line power balancing capability with a performance factor greater than a static proportional-integral (PI) and proportional-resonant (PR) controller. First, the controller capability is evaluated on a proof of concept aggregated power grid model or a single machine infinite bus system. Then, the tests for concurrently providing line balancing and voltage support are conducted by connecting SPIs at several locations on an unbalance three-phase IEEE 123 node distribution system model. It has been demonstrated that the proposed architecture is adaptable and performs better (3% to 5% improvement in error) when compared to static PI and PR controller during varying operating conditions.**

***Index Terms*—Adaptive control, *dq* control, minimum variance control, system identification, single-phase inverters (SPIs).**

I. Introduction

THREE-PHASE power distribution systems with unequal load distribution and unequal line impedances can cause phase current to unbalance, leading to voltage and current unbalance issues. The unbalanced nature of the current in each phase can be due to dissimilar single-phase loading and nonlinear loads. As the addition of distributed energy resources (DERs) based on renewable energy is on the rise, power flow on the distribution system varies between situations with phases. This condition combined with the reverse power flow from DERs can further worsen situations with voltage rise and other power quality issues. Most of the power generated from renewable energy resources (RERs) is injected into the distribution grid or delivered to the end-users through the use of power electronic converters [1]. At low-voltage distribution networks, conversion of power takes place via single-phase inverters (SPIs) [2]. The advantage of using SPIs over three-phase for unbalanced systems is that they can provide extra flexibility to control individual line power flows. The ability to inject and consume power by the grid-connected inverters (GCIs), can be used advantageously to control line power and provide voltage support for each phase. Power electronic converters and the flexible alternating current transmission system devices have already been designed [3] for voltage regulation and unbalance voltage mitigation. However, designating converters for the sole purpose of voltage regulation at various points in the power system is expensive. With the higher penetration of RERs, there would be a large number of these converters in the power distribution network [4], [5]. Previous research work has shown that phase balancing is possible using excess active power from the RERs or vice versa for active power curtailment [6]–[10], but this has its limitations especially when supplying power to satisfy demand is of the higher priority. A combination of active and reactive power to provide for the phase balancing has been explored in [11] but only by using static PI–based designs.

Recent advances in grid codes have made dynamic control of SPIs a necessity [12], [13]. However, such control is a difficult task as it requires considerable controller adaptation. The two extensively studied methods for controlling SPIs power output are the proportional resonant controller (stationary reference frame) and the PI controller (synchronous reference frame) [14]–[16]. The power output for grid-connected feedforward steady-state inverters is controlled by controlling the current at the output of the inverter. Current-controlled SPIs, usually use the PI controller with grid voltage feedforward as a decoupling term [14], [15]. The inability to track faster dynamic changes, creating steady-state errors and problems in tracking with background disturbance are the major drawbacks of the PI controllers [17], [18]. Also in synchronous reference frame modeling of the SPIs, there exists a coupling between the dq axis current, which can have a significant impact on the controller design methodology [14], [19]–[21]. One of the solutions to this

Manuscript received July 15, 2019; revised December 7, 2020 and February 16, 2020; accepted April 12, 2020. Date of publication May 13, 2020; date of current version July 1, 2020. Paper 2019-IACC-0989.R2, presented at the 2018 IEEE Industry Applications Society Annual Meeting, Portland, OR, USA, Sep. 23–27, and approved for publication in the IEEE TRANSACTIONS ON INDUSTRY APPLICATIONS by the Industrial Automation and Control Committee of the IEEE Industry Applications Society. This work was supported in part by by the U.S. Department of Energy's Office of Energy Efficiency and Renewable Energy (EERE) under the Solar Energy Technologies Office Award Number DE-EE0008774 and in part by the National Science Foundation ECS-1810174. *(Corresponding author: Sukumar Kamalasadan.)*

The authors are with the Energy Production Infrastructure Center and Department of Electrical Engineering, University of North Carolina at Charlotte, Charlotte, NC 28223 USA (e-mail: rbisht@uncc.edu; rbhattar@uncc.edu; ssubra17@uncc.edu; skamalas@uncc.edu).

Color versions of one or more of the figures in this article are available online at https://ieeexplore.ieee.org.

Digital Object Identifier 10.1109/TIA.2020.2994879

problem is by providing large gains to decrease the coupling effects [20], which can cause instability. Another approach by using filter inductor current state feedback is also used to decouple the dq axis current [21]. As inductor current state feedback (ICSF) eliminates techniques for the coupling caused by the digital delay, a one-step predicting ICSF (PRE-ICSF) was proposed in [22]. In this method, the step ahead predicted current is used to generate the decoupling term. However, both the ICSF and PRE-ICSF techniques are susceptible to parametric changes in the inverter. In [23] and [24], a complex vector-based controller is proposed to overcome parameter dependency of the previously mentioned techniques. However, the technique is applied to three-phase inverters. Another important factor is the problem related to frequency instability due to power imbalances. This issue is getting significant attention these days due to the increased number of single-phase loads.

This article presents a current control strategy based on system identification, which can be utilized for active and reactive control of SPIs to minimize the power imbalance in lines and provide voltage support. Also, in this work, the phase-shifting block to obtain the $\alpha - \beta$ component utilizes the grid frequency to obtain the actual 90° phase-shifted components. This leads to an orthogonal axis constructing method, which has a rapid dynamic response to the disturbance in the system that helps in independent active/reactive power control in an SPI. Additionally, the coupling issue in the single-phase inverter is minimized through the identification-based control, which tries to minimize the variance of the controlled variable from its set-point. The proposed dynamic controller design has a better response over the complete operating range of SPIs in the grid-connected mode as opposed to the conventional PI controllers. The proposed control method takes advantage of the well-known *dq* transformation, an analysis mostly employed for three-phase converters' analysis and control design. The system identification based adaptive minimum variance control also has a better dynamic response and disturbance rejection as compared to the conventional vector control [25], [26].

This article is an extended version of the author's earlier work [27]. It mainly focused on the following:

1) the dynamic power control and performance analysis of the adaptive controller with the conventional PI control,
2) power quality improvement and power unbalance mitigation, and
3) voltage regulation and unbalance mitigation.

The main theoretical and innovative contribution in this work is that the proposed architecture can balance line power as well as provided extra reactive power for voltage regulation using the power management control implemented in this article. Other main advantages of the proposed architecture are as follows.

1) The tuning of the controller is online and does not require the proper knowledge about the SPI parameters. This provides better tracking and dynamic stabilization.
2) The controller performs better during changing grid dynamics and DER output fluctuations.
3) The controller is adaptive, and any parametric changes that bring changes in power output of the inverter can be incorporated by the identification routine. It also provides flexibility to control powers in individual phases.
4) The method provides independent control on active and reactive power, which is beneficial for the consumer loads and ancillary services for the utility.

The rest of this article is organized as follows. Section II discusses the modeling of SPI. Section III discusses the system identification based adaptive control architecture. Section IV discusses the proof of concept demonstrates the scalability of the proposed controller. Section V discusses the application of the active and reactive power controlled single-phase GCIs for power balancing. The conclusions are deduced in Section VI.

II. Modeling and Design of SPI

Fig. 1 shows a typical structure of the single-phase voltage source inverter along with its control topology. The inverter uses active full-bridge topology that operates in all four quadrants of the PQ plane. For flexible control of active and reactive power, the *dq* reference frame based decoupled control technique is designed [15], [28], [29]. In this work, the dc side of the SPI is assumed to be connected to a battery energy storage system (BESS) and the dc link is assumed to be well regulated by the control system implemented in BESS.

A. Single-Phase dq Transformation

Single-phase system currents and voltages can be transformed into the $\alpha - \beta$ reference frame easily without any transformation matrix, unlike the three-phase system. For this purpose, the measured quantity is taken to be the α component and the β component is a 90° phase-shifted version of the measured quantity. The shift is computed through a phase-locked loop (PLL), which determines the frequency of the system[30]. The delay equivalent to the 90 ° phase shift is deduced from the system frequency. Hence, the $\alpha - \beta$ component of inverter current can be written as

$$\begin{bmatrix} i_{L\alpha} \\ i_{L\beta} \end{bmatrix} = \begin{bmatrix} i_{L(\omega t \mid \phi)} \\ i_{L\left(\omega t+\phi+\frac{\pi}{2}\right)} \end{bmatrix}. \tag{1}$$

The $\alpha - \beta$ component of inverter current is obtained and correspondingly the inverter current in the *dq* reference frame can be computed by

$$\begin{bmatrix} i_{Ld} \\ i_{Lq} \end{bmatrix} = \begin{bmatrix} \sin(\omega t) & -\cos(\omega t) \\ \cos(\omega t) & \sin(\omega t) \end{bmatrix} \begin{bmatrix} i_{L\alpha} \\ i_{L\beta} \end{bmatrix}. \tag{2}$$

The conversion technique can be utilized to generate the voltage components as well. With the appropriate voltage components, the signals can be used as feedback signals in the control loop, as shown in Fig. 1(b). The PLL helps in synchronizing the inverter output voltage with the grid voltage. This process helps in generating a clean sinusoidal modulation signal intended for the inverter switching. The PI controller inside the PLL improves the settling time and the damping factor for the transformed component. The PLL can also be used for monitoring changes in the grid voltage. The frequency obtained from PLL is utilized in computing the time delay to create a 90° phase shift and the angle

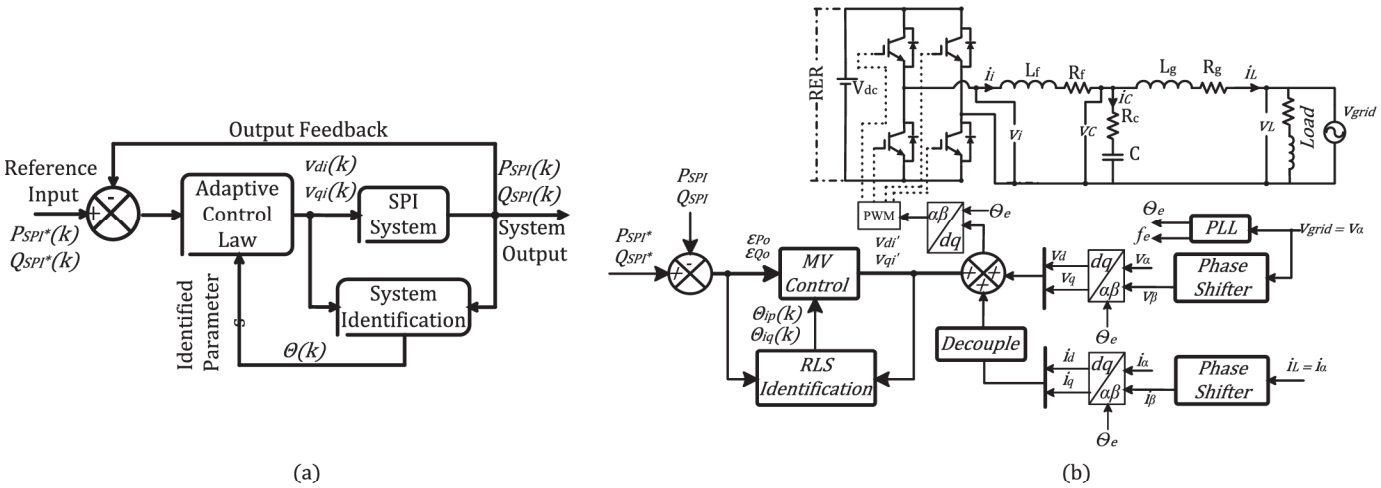

Fig. 1. Proposed adaptive control framework for grid-connected SPI. (a) General schematic. (b) Proposed implementation.

obtained from PLL provides the position of grid voltage vector with respect to the synchronously rotating reference frame.

B. Mathematical Model of SPI

Park's dq reference frame rotates synchronously with the inverter output voltage at angular speed ω_o. The current and voltage dynamics are represented by the following equations:

$$\frac{di_{\text{invd}}}{dt} = \frac{-R_f}{L_f} i_{\text{invd}} + \omega_o i_{\text{invq}} + \frac{1}{L_f}(v_{\text{invd}} - v_{dc}) \tag{3}$$

$$\frac{di_{\text{invq}}}{qt} = \frac{-R_f}{L_f} i_{\text{invq}} - \omega_o i_{\text{invd}} + \frac{1}{L_f}(v_{\text{invq}} - v_{qc}) \tag{4}$$

$$\frac{dv_{cd}}{dt} = \omega_o v_{cq} + \frac{1}{C_f}(i_{\text{invd}} - i_{Ld}) \tag{5}$$

$$\frac{dv_{cq}}{dt} = -\omega_o v_{cd} + \frac{1}{C_f}(i_{\text{invq}} - i_{Lq}) \tag{6}$$

$$\frac{di_{Ld}}{dt} = \frac{-R_g}{L_g} i_{Ld} + \omega_o i_{Lq} + \frac{1}{L_g}(v_{cd} - v_{Ld}) \tag{7}$$

$$\frac{di_{Lq}}{dt} = \frac{-R_g}{L_g} i_{Lq} - \omega_o i_{Ld} + \frac{1}{L_g}(v_{cq} - v_{Lq}). \tag{8}$$

Here, v_{invd}, v_{invq}, i_{invd}, and i_{invq} are the inverter's d- and q-axis output voltages and currents; v_{cd}, v_{cq}, i_{Ld}, and i_{Lq} represent the filter's d- and q-axis output voltages and currents; v_{Ld} and v_{Lq} are the d- and q-axis grid voltages. R_f, L_f, and C_f are the LC filter variables; and R_g and L_g are the resistance and inductance of the coupling inductor, respectively. From this, active and reactive power output of the inverter, P_{inv} and Q_{inv}, is given as

$$\begin{aligned} P_{\text{inv}} &= v_{Ld} i_{Ld} + v_{Lq} i_{Lq} \\ Q_{\text{inv}} &= v_{Ld} i_{Lq} + v_{Lq} i_{Ld}. \end{aligned} \tag{9}$$

With the rotating reference frame aligned with output voltage measured after the LC filter, the d-component is $v_{Ld} = V$ and the q-component $v_{Lq} = 0$, where V is the magnitude of output voltage vector. Hence, the active and reactive power output can be approximated by

$$\begin{aligned} P_{\text{inv}} &= v_{Ld} i_{Ld} \\ Q_{\text{inv}} &= v_{Ld} i_{Lq}. \end{aligned} \tag{10}$$

Generalizing (3)–(10), we get the following state-space form

$$\begin{aligned} \Delta \dot{x} &= \mathbf{A}\Delta x + \mathbf{B}\Delta u \\ \Delta y &= \mathbf{C}\Delta x \end{aligned} \tag{11}$$

where

$$\begin{aligned} \Delta x &= \begin{bmatrix} \Delta i_{\text{invd}} & \Delta i_{\text{invq}} & \Delta v_{cd} & \Delta v_{cq} & \Delta i_{Ld} & \Delta i_{qL} \end{bmatrix}^T \\ \Delta u &= \begin{bmatrix} \Delta v_{\text{invd}} & \Delta v_{\text{invq}} \end{bmatrix}^T \\ \Delta y &= \begin{bmatrix} \Delta Q_{\text{inv}} & \Delta Q_{\text{inv}} \end{bmatrix}^T. \end{aligned}$$

$\mathbf{A}$, $\mathbf{B}$, and $\mathbf{C}$ are the system state, input, and output matrices, respectively, as given in (12)

$$\mathbf{A} = \begin{bmatrix} -\frac{R_f}{L_f} & \omega_o & -\frac{1}{L_f} & 0 & 0 & 0 \\ \omega_o & -\frac{R_f}{L_f} & 0 & -\frac{1}{L_f} & 0 & 0 \\ \frac{1}{C_f} & 0 & 0 & \omega_o & -\frac{1}{C_f} & 0 \\ 0 & \frac{1}{C_f} & -\omega_o & 0 & 0 & -\frac{1}{C_f} \\ 0 & 0 & \frac{1}{L_g} & 0 & -\frac{R_g}{L_g} & \omega_o \\ 0 & 0 & 0 & \frac{1}{L_g} & -\omega_o & -\frac{R_g}{L_g} \end{bmatrix},$$

$$\mathbf{B} = \begin{bmatrix} \frac{1}{L_f} & 0 & 0 & 0 & 0 & 0 \\ 0 & \frac{1}{L_f} & 0 & 0 & 0 & 0 \end{bmatrix}^T,$$

$$\mathbf{C} = \begin{bmatrix} 0 & 0 & 0 & 0 & v_{Ld} & 0 \\ 0 & 0 & 0 & 0 & 0 & v_{Ld} \end{bmatrix}. \tag{12}$$

C. Inverter Control Design Based on PI Control

The GCI has the grid-side voltage maintained as shown in (10). From this, one can control the active and reactive power

TABLE I
PI CONTROLLER DESIGN AND GAINS

Control Loop	PI Tuned Based on	K_p Gain	K_i Gain
Outer: Power	SMIB	0.3	1
Inner: Current	SMIB	0.7	10
Outer: Power	IEEE 123 bus system	0.8	3
Inner: Current	IEEE 123 bus system	10	30

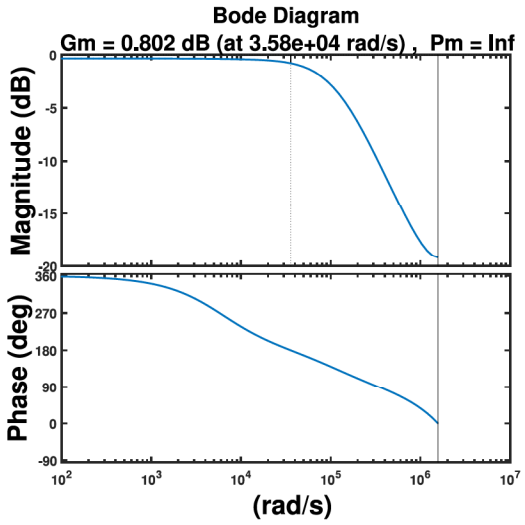

Fig. 2. Bode plot of the closed-loop system.

by controlling i_{Ld} and i_{Lq}, and further, the control action propagates to the modulating waveform by changing the output voltage v_{cd} and v_{cq}. v_{cd} and v_{cq} can be changed by changing the inverter output voltage $v_{\text{inv}d}$ and $v_{\text{inv}q}$, respectively. For designing a conventional PI control, (11) and (12) are first converted into a transfer function form. The discrete model representation can then be written as (assuming a third-order approximation)

$$\frac{i_{\text{inv}dq,k} - i_{\text{inv}dq,k-1}}{Ts} = -\frac{R_f}{L_f}\left(\frac{i_{\text{inv}dq,k} - i_{\text{inv}dq,k-1}}{2}\right) - \omega_o \frac{i_{\text{inv}dq,k} - i_{\text{inv}dq,k-1}}{2} + \frac{1}{L_f}\left(v_{\text{inv}dq,k-1} - v_{dc,k-1}\right) \quad (13)$$

where Ts is the sampling of the simulation and, k is the current or kth sample of the respective parameter. Either using the discretized (11) or the zero-order hold representation, the controller can be tuned. A tuning method based on phase and gain margins [31] (see Fig. 2), is used for tuning the PI controller. Table I shows the PI control gains for simulation purposes. Plots in Fig. 2 shows the designed gain and phase margins.

III. ADAPTIVE CONTROL OF AN SPI

Fig. 1 presents the schematic of an adaptive control system implemented on an SPI. The adaptive controller comprises of the following three main components:

1) the plant to be controlled;
2) system identifier;
3) controller-based on identified system parameters.

Based on how the power variables are related to the inverter output voltage, presented in Section II, the system is represented by a third-order polynomial that is processed by the identifier. The design of the system identifier and the minimum variance adaptive control is presented as follows.

A. Recursive Least Squares Estimation

The z-domain transfer function parameters of the SPI system are identified every sample period "k" using the input signal "$v_{\text{inv}d}(k)$" and output signal "$P_{\text{inv}}(k)$" of the system. The system can be represented by a third-order z-domain transfer function of the following form for active power control loop:

$$\frac{P_{\text{inv}}(k)}{v_{\text{inv}d}(k)} = \frac{b_0 z^{-1} + b_1 z^{-2} + b_1 z^{-3}}{1 + a_1 z^{-1} + a_2 z^{-2} + a_3 z^{-3}} = \frac{B(z^{-1})}{A(z^{-1})} \quad (14)$$

which in turn can be represented by a difference equation form for sample "k" as

$$P_{\text{inv}}(k) = -a_1 P_{\text{inv}}(k-1) - a_2 P_{\text{inv}}(k-2) - a_3 P_{\text{inv}}(k-3) + b_0 v_{\text{inv}d}(k-1) + b_1 v_{\text{inv}d}(k-2) + b_2 v_{\text{inv}d}(k-3). \quad (15)$$

Similarly for sample "$k-N+1$"

$$P_{\text{inv}}(k-N+1) = -a_1 P_{\text{inv}}(k-N) - a_2 P_{\text{inv}}(k-N-1) - \cdots - a_3 P_{\text{inv}}(k-N-2) + b_0 v_{id}(k-N) + \cdots + b_1 v_{id}(k-N-1) + b_2 v_{id}(k-N-2). \quad (16)$$

"N" is the observation length and the group of difference equations (15) and (16) can be written in the following matrix form:

$$\overbrace{\begin{bmatrix} P_{\text{inv}}(k) \\ P_{\text{inv}}(k-1) \\ \vdots \\ P_{\text{inv}}(k-N+1) \end{bmatrix}}^{N\times 1}_{\Phi_{\text{model}}} = \overbrace{[X]}^{N\times 6} \overbrace{\begin{bmatrix} a_1 \\ \vdots \\ a_3 \\ b_0 \\ \vdots \\ b_2 \end{bmatrix}}^{6\times 1}_{\Theta} \quad (17)$$

where X is given by (18) shown at the bottom of this page.

$$X = \begin{bmatrix} -P_{\text{inv}}(k-1) & . & -P_{\text{inv}}(k-3) & v_{\text{inv}d}(k-1) & . & v_{\text{inv}d}(k-3) \\ -P_{\text{inv}}(k-2) & . & -P_{\text{inv}}(k-4) & v_{\text{inv}d}(k-2) & . & v_{\text{inv}d}(k-4) \\ \cdots & . & \cdots & \cdots & . & \cdots \\ \cdots & . & \cdots & \cdots & . & \cdots \\ -P_{\text{inv}}(k-N) & . & -P_{\text{inv}}(k-N-2) & v_{\text{inv}d}(k-N) & . & v_{\text{inv}d}(k-N-2) \end{bmatrix} \quad (18)$$

The error between the actual system and the system model is given by "ϵ"

$$\epsilon = \Phi_{\text{system}} - \Phi_{\text{model}} \tag{19}$$

where Φ_{system} is the vector of measured system output variables.

From (17), $\Phi_{\text{model}} = X \cdot \Theta$ can be substituted in (19) to get

$$\epsilon = \Phi_{\text{system}} - X \cdot \Theta. \tag{20}$$

The basis of the least squares identification is to minimize the square of the error "ϵ" for which a criterion "J" is defined as

$$J = \epsilon^t \epsilon = \sum_{i=k}^{k+N} \epsilon^2. \tag{21}$$

On minimizing the criterion "J," the system parameters "Θ" representing the parameter vector is solved and the following form of equation for "Θ" is obtained

$$\Theta(k) = \Theta(k-1) + K(k)\left[\Phi(k) - X^t(k)\Theta(k-1)\right] \tag{22}$$

where

$$K(k) = \frac{P(k-1)X(k)}{\gamma + X^t(k)P(k-1)X(k)} \tag{23}$$

$$P(k) = \frac{\left[I - K(k)X^t(k)\right]P(k-1)}{\gamma} \tag{24}$$

where $K(k)$ is the Kalman filter gain, $P(k)$ is the covariance matrix of the error during the estimation of parameter vector Θ, which has the size of 6×6 , I is the identity matrix of size 6×6 , and γ is the forgetting factor.

Once Θ is solved using (22), the parameters $a_1, a_2, \ldots, a_3, b_0, b_1, \ldots, b_2$ that define the third-order transfer function model of the system can be obtained. Once the parameters are obtained, the controller can be designed using the identified parameters.

B. Minimum Variance Control

In this section, the design methodology of the minimum variance controller is discussed. The minimum variance controller is a digital control technique utilizing the parameters of the transfer function representing the system along with the past inputs and outputs. The goal of the minimum variance controller is to closely regulate the active and reactive power of the SPI by generating the proper voltage sequence to generate pulsewidth modulation pulses. The derivation of the minimum variance control law for the active power output of the inverter is shown below and a similar process is followed for the control law derivation of the reactive power. For the minimum variance control design, the system is assumed to be described by the controlled auto regressive moving average (CARMA) model, i.e.,

$$\epsilon_{P_o}(k) = \frac{B(z^{-1})}{A(z^{-1})} \times v'_{\text{invd}}(k) + \frac{C(z^{-1})}{A(q^{-1})} \times \varrho(k) \tag{25}$$

where $\epsilon_{P_o}(k) = P^*_{\text{inv}}(k) - P_{\text{inv}}(k)$, $P^*_{\text{inv}}(k)$ is the reference active power to be delivered to the grid, $P_{\text{inv}}(k)$ is the actual active power being delivered, v'_{invq} is the q-axis voltage sequence applied at $k\text{th}$ instant in time in the inverter, ϱ is the error in the model representation.

The CARMA model is used in the proposed design, as this representation has some level of uncertainty and randomness built-in, which consider the future correlation of the inverter with past responses. The assumption is valid as the inverter operation in the power system has similar behavior. Moreover, the moving average part will filter or smooth out any short term irregularity or inconsistencies in the data series, which helps in obtaining a smoother model of the system. White noise modeling for estimation error is included as it is assumed that the estimation error is independent of past errors and there is no autocorrelation of the estimation error with its past terms. This is also a valid assumption. Based on the system time delay information, the minimum variance controller minimizes the variance of the output at $k+d$ with respect to the expected value of output at $k+d$ using the information gathered at up to time instant k, i.e, the controller goal is to minimize the following objective function:

$$J(k) = E_x\{\epsilon_{P_o}(k+d)^2\}$$

where d is the assumed system delay and E_x represents the expected value of the output d steps into the future, which in this case is zero.

Based on the derivation of the relation between power variables and inverter output voltages in Section II, a third-order linear representation of the system is selected. This can be represented as

$$\begin{aligned} A(z^{-1})\epsilon_{P_o}(k) &= B(z^{-1})v'_{\text{invd}}(k) + C(z^{-1})\varrho(k) \\ A(z^{-1}) &= 1 + a_1 z^{-1} + a_2 z^{-2} + a_3 z^{-3} \\ B(z^{-1}) &= b_0 z^{-1} + b_1 z^{-2} + b_2 z^{-3} \\ C(z^{-1}) &= 1. \end{aligned} \tag{26}$$

From the system equation in (26), it can be observed that

$$\begin{aligned} \epsilon_{P_o}(k) &= -a_1 z^{-1}\epsilon_{P_o}(k) - a_2 z^{-2}\epsilon_{P_o}(k) - a_3 z^{-3}\epsilon_{P_o}(k) \\ &+ b_0 z^{-1} v'_{\text{invd}}(k) + b_1 z^{-2} v'_{\text{invd}}(k) + b_2 z^{-3} v'_{\text{invd}}(k) + \varrho(k). \end{aligned} \tag{27}$$

Now, if the time index in prediction is shifted by one, (27) can be written as

$$\begin{aligned} \epsilon_{P_o}(k+1) &= -a_1\epsilon_{P_o}(k) - a_2\epsilon_{P_o}(k-1) - a_3\epsilon_{P_o}(k-2) \\ &+ b_0 v'_{\text{invd}}(k) + b_1 v'_{\text{invd}}(k-1) + b_2 v'_{\text{invd}}(k-2) + \varrho(k+1). \end{aligned} \tag{28}$$

The left-hand side of (28) represents the output signal, and it is one time step ahead. The right-hand side has the information about the present and past output signal, present and past input signal and future model estimation error. The control action $v'_{\text{invq}}(k)$ is computed in order to optimize the variance of the output one step ahead in the future as

$$\begin{aligned} \underset{v'_{\text{invd}}(k)}{\text{Min}}\{J(k)\} &= \underset{v'_{\text{invd}}(k)}{\text{Min}} E_x\{\epsilon_{P_o}(k+1)^2\} \\ &= \underset{v'_{\text{invd}}(k)}{\text{Min}} E_x\{[(-a_1)\epsilon_{P_o}(k) + (-a_2)\epsilon_{P_o}(k-1) + (-a_3)\epsilon_{P_o}} \end{aligned}$$

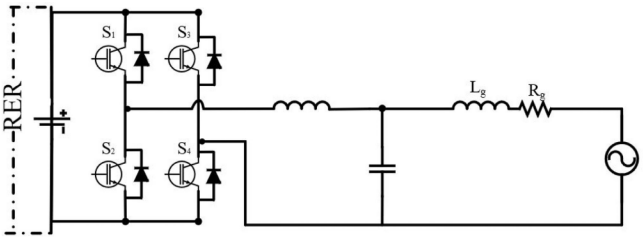

Fig. 3. SMIB test system for the SPI.

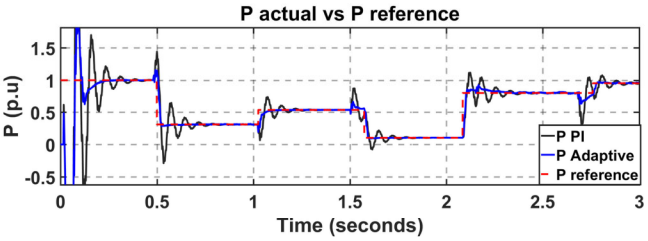

Fig. 4. Case 1 for OMIB: Active power tracking performance comparison.

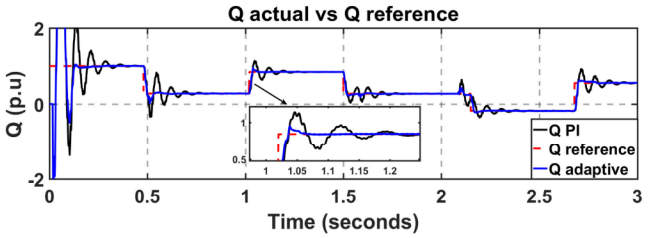

Fig. 5. Case 1 for OMIB: Reactive power tracking performance comparison.

$$(k-2)+(b_0)v'_{\text{inv}d}(k)+(b_1)v'_{\text{inv}d}(k-1)+(b_2)v'_{\text{inv}d}$$
$$(k-2)+\varrho(k+1)]^2\}. \quad (29)$$

Equation (29) contains present and past inputs, present and past outputs, and future model estimation error. The estimation error is assumed as white noise, and its future values cannot be correlated with past and/or present signals. Hence, one can achieve the minimum variance when the sum of the first six components is set to zero, i.e.,

$$-a_1\epsilon_{P_o}(k)-a_2\epsilon_{P_o}(k-1)-a_3\epsilon_{P_o}(k-2)$$
$$+b_0v'_{\text{inv}d}(k)+b_1v'_{\text{inv}d}(k-1)+b_2v'_{\text{inv}d}(k-2)=0. \quad (30)$$

The minimum variance control law for active power control is given by

$$v'_{\text{inv}d}(k)=(a_1\epsilon_{P_o}(k)+a_2\epsilon_{P_o}(k-1)+a_3\epsilon_{P_o}(k-2)$$
$$-b_1v'_{\text{inv}d}(k-1)-b_2v'_{\text{inv}d}(k-2))/b_0. \quad (31)$$

Similarly, the minimum variance control law for reactive power control is given by

$$v'_{\text{inv}q}(k)=(a_1\epsilon_{Q_o}(k)+a_2\epsilon_{Q_o}(k-1)+a_3\epsilon_{Q_o}(k-2)$$
$$-b_1v'_{qi}(k-1)-b_2v'_{qi}(k-2))/b_0. \quad (32)$$

where $\epsilon_{Q_o}(k)=Q^*_{\text{inv}}(k)-Q_{\text{inv}}(k)$. Q^*_{inv} is the reference reactive power to be delivered to the grid and Q_{inv} is the actual reactive power delivered. Fig. 1(a) represents the overall control structure proposed in this work for active and reactive power control of single-phase GCI. The system identification sampling time and controller sampling time used in this work are provided in the Appendix.

IV. Controller Performance Comparison

The adaptive minimum variance controller performance validation was carried out on a single-phase GCI, in a one/single machine infinite bus (OMIB/SMIB) setup as shown in Fig. 3. This is to provide a proof of concept for the adaptation on active and reactive power control on one SPI. This proof of concept paves way for scaling to a larger system to perform various tests with a real grid model. The performance comparison of the controller is based on digital simulation. The simulation results presented are with the nonlinear switching model of the inverters for the different types of controllers compared. The linearized model was primarily used to simplify the control design.

A. Proof of Concept: OMIB

The dc module consists of a photovoltaic (PV) battery system rated for 1.5 kW and 1000 V dc with the ac side connected to a constant voltage source or infinite bus at 230 V. The comparative studies are performed for the PI and the adaptive controller based on active and reactive power tracking capability under varying grid conditions.

1) Case 1: Active and Reactive Power Tracking With Arbitrary References: Figs. 4 and 5 compare the active and reactive power reference tracking performance of the proposed controller with the conventional PI controller. PI controller for the SPI has been tuned based on the system state-space model presented in (11) and (12). The controller is optimized to have an overshoot of less than 20% for step changes and with a settling time of 0.1 s. It can be observed from Figs. 4 and 5 that the proposed controller has a better dynamic response in terms of less overshoot and lower settling time as compared to the conventional PI-based control. Also, note that the proposed controller did not assume prior knowledge of the system parameters as opposed to the PI controller, which required prior knowledge of the system parameters for proper controller tuning. The results show that the proposed system identification based control can be a better alternative to the existing vector control scheme for the SPI.

2) Case 2: Controller Performance During Voltage Sag: Fig. 6 presents the active and reactive power graphs with a presence of voltage sag on the grid at the 1.5-s mark. The voltage sag is on the grid side, which is a 10 cycle sag that lowers the grid voltage from 0.99 to 0.8 p.u. When the sag occurs, the low-voltage ride-through capability of the inverter tries to keep tracking the power output reference. Observation from the figure shows that the capability of the adaptive technique is comparable to the PI control. Active power overshoot with the conventional PI control is much larger compared to the adaptive controller and shows better convergence to the setpoint during and after the sag.

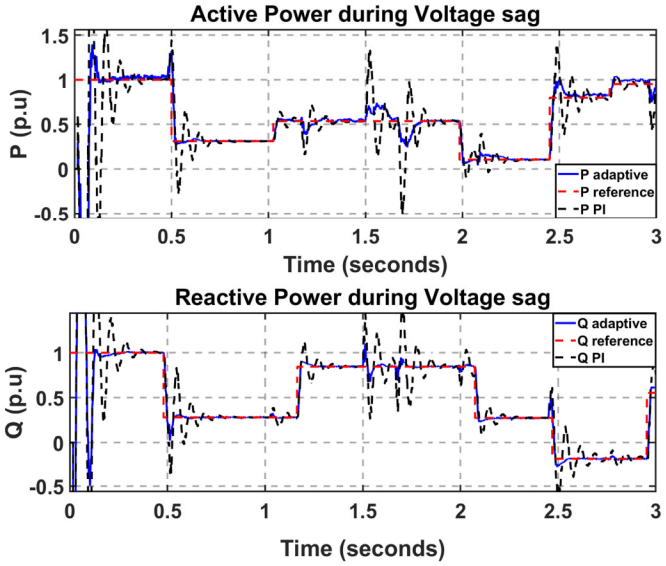

Fig. 6. Case 2 for OMIB: Active and reactive power comparisons during voltage sag.

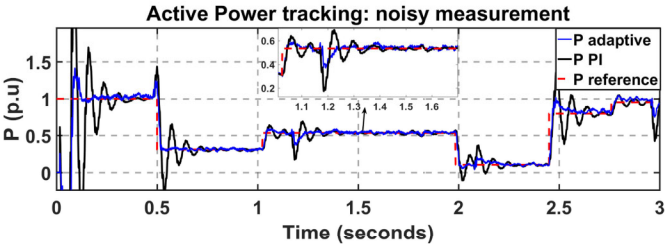

Fig. 7. Case 3 for OMIB: Active Power comparisons when feedback noise is introduced.

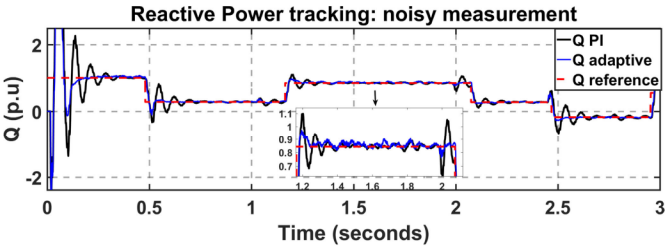

Fig. 8. Case 3 for OMIB: Reactive power comparison when feedback noise is introduced.

3) Case 3: Controller Performance With Measurement Noise: Adaptive control is dependent on the measurement of the system's input and output data. Any variations and noise in the measurements can cause the controller to malfunction and compromise the power tracking capability. Therefore, a test is performed in the presence of the noise in the measurements. Figs. 7 and 8 show the active and reactive power tracking or the PI and adaptive controller in the presence of the measurement noise. The minimum variance adaptive controller has a better steady-state tracking performance than that of the conventional PI in the presence of measurement noise. This feature is crucial as the feedback measurements can include noises coming from inverter switching, fast changes from the load and, generation sources like PV.

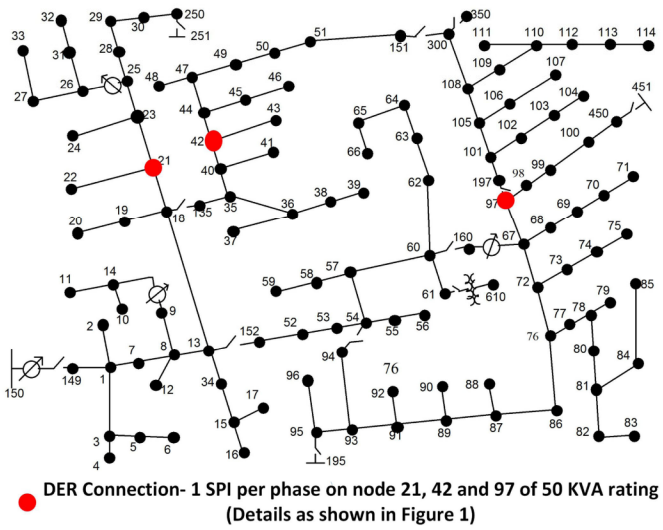

Fig. 9. Modified IEEE 123-bus system.

B. Scalability: Study With IEEE 123 Bus system

The scalability of the proposed architecture is tested using a modified IEEE 123 Node Test Feeder (see Fig. 9). The power distribution system from [32] is modified to include DER connected SPI's as indicated in Fig. 9. The nature of this system is that it is inherently unbalanced. So the application chosen is power and voltage balancing. The *dq* based SPI controller with the proposed architecture is connected to bus 21 (inverters 504, 505, and 506), bus 42 (inverters 501, 502, and 503), and bus 97 (inverters 507, 508, and 509) on all the three phases (total nine inverters). The inverters have a power rating of 50 kW at 2.4 kV. The power balancing is based on (32) and (33). For comparison purposes, two controllers are used. First, PI controllers are used with retuned best parameters based on the same process discussed in Section II-C. Also, a PR controller is designed for comparison purposes. The PR controller is based on the basic controller formulation shown in [33]. The control signals were adapted to the control architecture shown in Fig. 1 for a clear comparison in the $\alpha\beta$ reference frame. In the following section, the simulation results showcased are for inverter 501. This is because, the other inverters (502–509) portray a similar dynamic response to the changes provided, as seen in the following cases.

1) Case 1: Active and Reactive Power Tracking With DERs Attached to the 123-Bus System: Two subcases are illustrated in this case. In Case (a), tracking ability of active and reactive power of the proposed controller compared to PI gains tuned based on SMIB is illustrated. Fig. 10 compares the tracking performance of the PI, PR, and adaptive controllers. Inverter 501 attached to bus 42 is taken as the reference. It can be seen that PI and PR control for the SPI's active and reactive power control is comparable in tracking the references provided to the outer loop. However, when connected to the IEEE 123 bus system their performance deteriorated. The adaptive control,

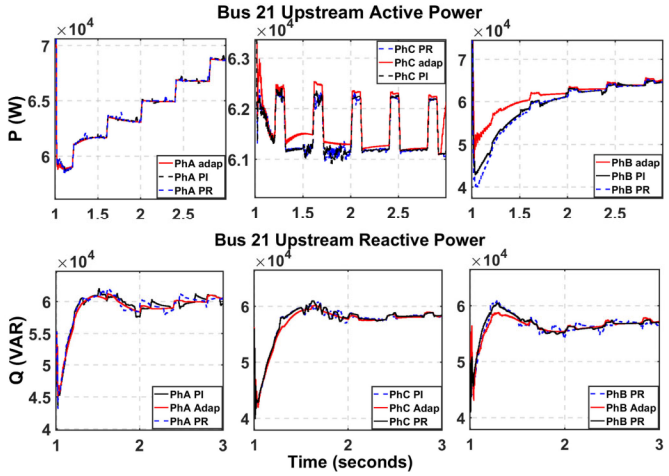

Fig. 10. Case 1 for unbalanced application: Bus 21 active and reactive power balancing capability comparisons

TABLE II
PERFORMANCE ANALYSIS OF CASE 2 OF SYSTEM SCALIBILITY AND CASE 3 OF OMIB IN SECTION IV

Controller	Steady State %error P	Steady State %error Q	% Improvement w.r.t OMIB PI control
Case 2			P & Q
OMIB PI	15%	10%	
PI	3.6%	5%	76% 50%
PR	4%	5.6%	73% 44%
Adaptive	3%	4.2%	80% 58%
Case 3			P & Q
PI	1.35%	3.5%	91% 50%
Adaptive	1.26%	3%	65% 70%

on the other hand, has a better performance comparatively. Quantitative comparisons are shown in Table II. In Case (b), active and reactive power tracking are compared with PI gains based on the IEEE 123-bus system configuration (see Fig. 11). It can be seen that the proposed adaptive control architecture has similar characteristics but faster convergence, lower under and overshoot, and flexibility of implementation to any generic inverter topology. This is also exemplified by the results in Table II.

2) Case 2: Active and Reactive Power Tracking During Voltage Sag: Fig. 12 shows the active and reactive power comparison during the presence of a grid voltage sag where the grid voltage goes from 0.99 to 0.8 p.u at 2.5 s. It can be observed that the adaptive controller has a good low-voltage ride-through capability and shows better convergence to the setpoint once the sag is cleared.

3) Case 3: Active and Reactive Power Tracking Under Oscillatory Reference Change and Voltage Sag: Fig. 13 shows the tracking performance of the PI and proposed controller under random oscillatory reference and voltage sag conditions similar to that of Case 2. In this case, even though the active power tracking is comparable with PI-controller, the proposed architecture shows the better performance in active and reactive power tracking.

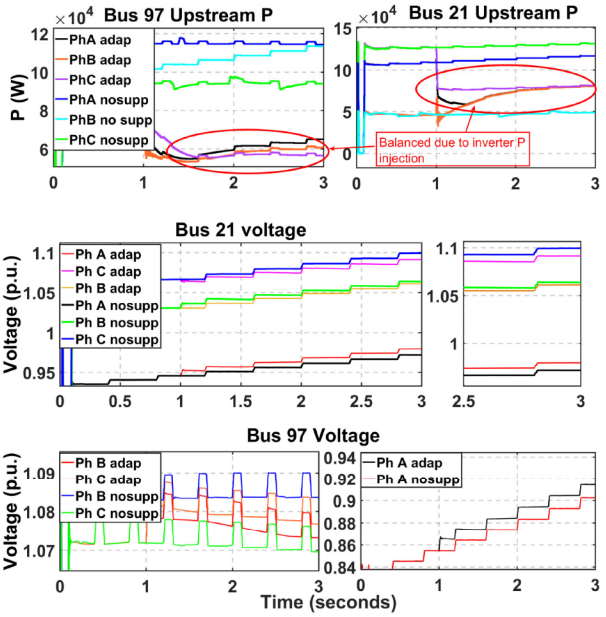

Fig. 11. Case 2 for unbalanced application: Bus 21 and 97 upstream Active-Reactive Power and Voltage after voltage balancing provided by the inverter and their respective Bus voltages.

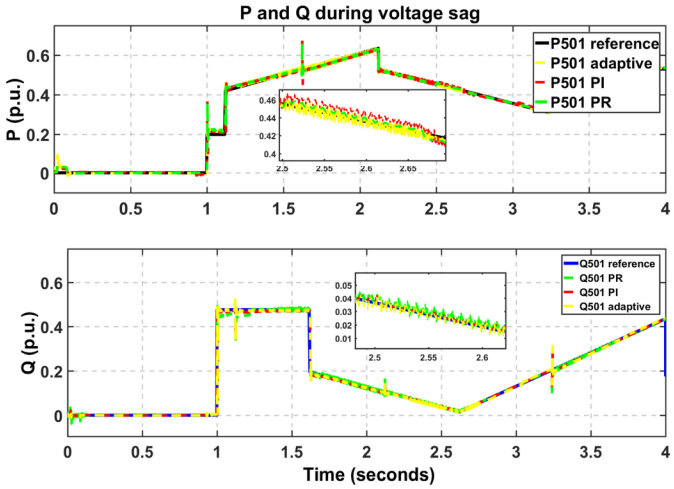

Fig. 12. Case 2: System scalability: Active and reactive power tracking comparisons during voltage sag with PR and re-tuned PID parameters.

Table II summarizes the quantitative analysis of the controller performance compared to the retuned PI and PR controllers for scalibility and OMIB studies. Steady-state error was determined after 20 ms of any form of perturbation given to the reference set-points; so that each controller can be compared on an equal criterion. It can be seen that the proposed architecture shows the superior performance when compared to other controllers.

V. APPLICATION TO UNBALANCED THREE-PHASE SYSTEMS

Reactive power generation by inverters is a valuable commodity for the grid, and controlling the inverter output powers can help quench some of the issues related to voltage dynamics. In this section, the focus is on utilizing the proposed architecture to

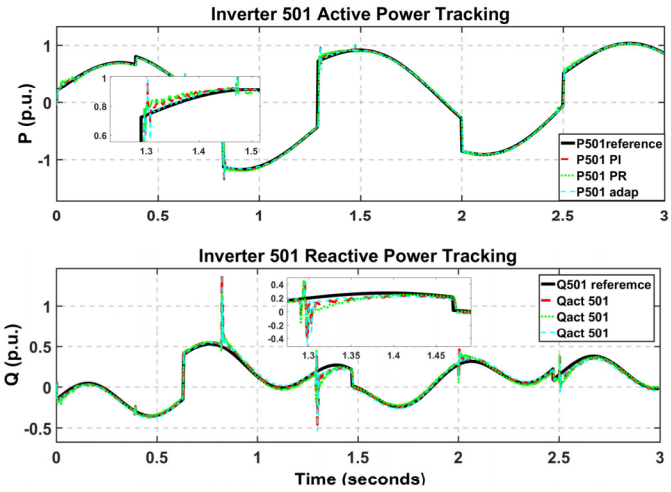

Fig. 13. Case 3: System scalability: Active and reactive power tracking comparisons during voltage sag with varying reference PR and re-tuned PID parameters.

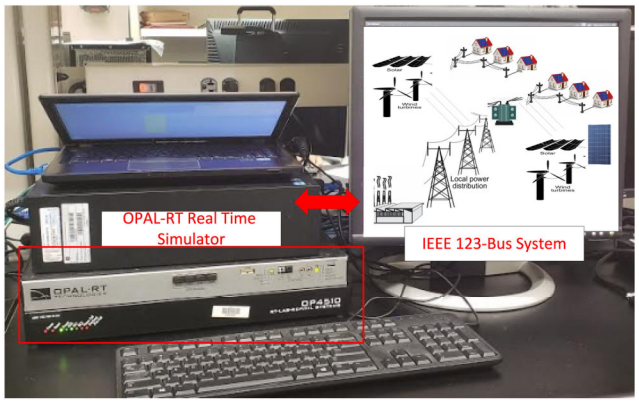

Fig. 14. Real-time hardware test bed for the studying IEEE 123-bus system.

mitigate the power unbalance and improve voltage dynamics and deviations from the nominal voltage. The application of inverter control in unbalanced systems is performed using the OPAL-RT RT-lab setup as shown in Fig. 14. Here the IEEE 123 bus system is simulated in the OP4510 real-time simulator, which in the future will provide a base setup for power hardware in the loop simulations. The following cases in the following section are performed in the RT-lab testbed.

A. Case 1: Phase Power Balancing With Adaptive Controlled SPIs

For this study nodes 42, 21, and 97 have single-phase grid-tied inverters as shown in Fig. 9. These inverters can control the output active and reactive powers flowing out of the GCIs. To control or dictate the power generation, the references are created by using the upstream power. For this purpose, buses 42, 21, and 97 have power meters connected, which measures active power and the voltage. Here, P_a, P_b and P_c, Q_a, Q_b, and Q_c are the active and reactive power flowing through each phase. The setpoint is the average power calculated using (33 and (34). Here, $P_{\text{inv}a}$ and $Q_{\text{inv}a}$ represent active and reactive power output

TABLE III
PERFORMANCE ANALYSIS OF CASE 1 IN SECTION V

Controller	Steady State %error P	Steady State %error Q	% Improvement w.r.t PI control
Inverters at Bus 42			P & Q
PI	1.84%	3.43%	
Adaptive	0.6%	1.2%	71% 65%
PR	2.1%	3.8%	
Inverters at Bus 21			
PI	2%	2.42%	
Adaptive	0.56%	0.89%	72% 63%
PR	2.3%	4%	
Inverters at Bus 97			
PI	1.72%	2.6%	
Adaptive	0.68%	0.91%	60% 65%
PR	2%	3%	

of the inverter attached to phase a and P_{aref} and Q_{aref} are power references for the same inverter. Similarly, these references can be generated for the inverters on the other two phases as well. For the following cases, the inverters start to participate at the 1-s mark of simulation time

$$\frac{(P_a + P_b + P_c)}{3} - P_{\text{inv}a} = P_{\text{aref}} \tag{33}$$

$$\frac{(Q_a + Q_b + Q_c)}{3} - Q_{\text{inv}a} = Q_{\text{aref}}. \tag{34}$$

When the GCIs intervene, the active and reactive powers seen upstream converge and stabilize the average value of the active and reactive power, respectively. It can be seen that the phase power is not balanced. In Fig. 10, "P PI" and "P adap" curves show the upstream powers when the powers are supported with SPIs. Please note that simulation results in Fig. 10 only show bus 21 results, as the other two buses show similar behavior. It can be seen that the power from the adaptive controlled SPIs shows better tracking and balancing as opposed to PI. This can further help in regulating the voltage, as removing power unbalance from the system improves the overall system's stability. The adaptive controller from Fig. 10, has a smoother transition toward balancing out the upstream reactive powers than the PI controller. This steady-state error does not show in the traditional active and reactive power tracking but when there is a supervisory or an extra controller driven setpoint generation, the performance deteriorates. The adaptive controller steady-state error for active and reactive power tracking is 0.56% and 0.89%, respectively, which is an improvement of 71% and 63% from PI control. The steady-state errors are observed after 20 ms of perturbation or reference set-point change so that each controller efficiency is judged based on equal criterion as explained earlier. The performance analysis of the proposed control architecture is summarized in Table III. It can be seen that with the proposed architecture an improvement in performance of more than 50% is achieved.

B. Case 2: Voltage Unbalance Mitigation

In this case, the voltage is monitored and corrected by the inverter at the point of common coupling. The error generated

TABLE IV
PERFORMANCE ANALYSIS OF CASE 2 IN SECTION V

Control	Steady State Voltage %error	% Improvement w.r.t PI control
Bus 21		
PI	0.29%	
Adaptive	0.28%	3.4%
Bus 42		
PI	0.2%	
Adaptive	0.185%	7%
Bus 97		
PI	0.25%	
Adaptive	0.24%	4%

by the measured voltage with the required reference is provided to the reactive power loop of the inverter. The voltage control loop has a PI controller that takes the voltage error as the input and generates the corresponding q-axis current reference for the inner loop. As seen in (10), the reactive power generation depends on the d-axis voltage and the q-axis current at the LC filter. The required reactive power for complete mitigation or balancing voltage might be different or higher than the rating of the inverter, but having the GCI help regulate the voltage up to the rated capacity of the GCI is the main objective here. Our single-phase DER inverter system is rated for 50 kW, therefore, when there is no active power demand, theoretically, the reactive power support by the GCI can be up to 50 kVAR. It can be seen from Fig. 11 that the proposed architecture can improve the voltage very effectively. Table IV shows the qualitative improvement when compared to the PI controller. It can be seen that a minimum of 3% overall improvement in the voltage can be attained.

VI. CONCLUSION

This article presents power and voltage unbalance mitigation methodology, provided by an adaptive minimum variance control based single-phase GCI. First, the model of the SPI in the grid following mode and the design of the proposed controller is illustrated. The adaptive control shows the better dynamic performance and noise rejection capability compared to the conventional PI control for an SMIB system. The proposed controller can adapt to the system topology change, unlike the PI controller, whose gains have to be retuned depending on the system. The control architecture is simple and allows flexible active and reactive control for the SPI. Second, the article presents a method to help mitigate the unbalanced nature of the three-phase system through the contribution of these SPIs. Using the active and reactive power control ability of the SPIs, the line power unbalance is mitigated completely. Third, this article presents the power and voltage balancing method using the readily available reactive power of the SPI to minimize the voltage error and improve the voltage profile of the system in conjunction with the active line power balancing. The overall advantage and novelty are that the proposed architecture can be used for coordinated multiple point active and reactive power support for the power distribution system.

APPENDIX

VA rating of SPI = 50 kVA, rated voltage = 2401 V, $R_f = 10^{-3}\,\Omega$, $L_f = 10^{-3}$ H, $R_c = 10^{-4}\,\Omega$, $C = 6.6\,\mu$F, $L_g = 10^{-2}$ H, $R_g = 0.033\,\Omega$, dc-link voltage = 1000 V, grid nominal frequency = 60 Hz, inverter swictching frequency = 20 kHz. System identification time step = 0.5 ms. MVC control time step = 5 ms.

REFERENCES

[1] H. A. Rahman, M. S. Majid, A. R. Jordehi, G. C. Kim, M. Y. Hassan, and S. O. Fadhl, "Operation and control strategies of integrated distributed energy resources: A review," *Renewable Sustain. Energy Rev.*, vol. 51, no. Suppl. C, pp. 1412–1420, 2015.

[2] J. Jana, H. Saha, and K. D. Bhattacharya, "A review of inverter topologies for single-phase grid-connected photovoltaic systems," *Renewable Sustain. Energy Rev.*, vol. 72, no. Suppl. C, pp. 1256–1270, 2017.

[3] M. Y. Suliman and M. Emad Farrag, "Power balance and control of transmission lines using static series compensator," in *Proc. 53rd Int. Univ. Power Eng. Conf.*, Sep. 2018, pp. 1–5.

[4] M. Zeraati, M. E. Hamedani Golshan, and J. M. Guerrero, "Distributed control of battery energy storage systems for voltage regulation in distribution networks with high PV penetration," *IEEE Trans. Smart Grid*, vol. 9, no. 4, pp. 3582–3593, Jul. 2018.

[5] S. Weckx and J. Driesen, "Load balancing with EV chargers and PV inverters in unbalanced distribution grids," *IEEE Trans. Sustain. Energy*, vol. 6, no. 2, pp. 635–643, Apr. 2015.

[6] X. Su, M. A. S. Masoum, and P. J. Wolfs, "Optimal PV inverter reactive power control and real power curtailment to improve performance of unbalanced four-wire LV distribution networks," *IEEE Trans. Sustain. Energy*, vol. 5, no. 3, pp. 967–977, Jul. 2014.

[7] B. A. Robbins, C. N. Hadjicostis, and A. D. Domínguez-García,"A two-stage distributed architecture for voltage control in power distribution systems, "*IEEE Trans. Power Syst.*, vol. 28, no. 2, pp. 1470–1482, May 2013.

[8] I. E. Saad, N. H. Saad, and W. A. S. El-Khattam, "Optimal unbalance mitigation for three-phase distribution networks equipped with single-phase PV systems," in *Proc. 28th Int. Middle East Power Syst. Conf.*, Dec. 2018, pp. 980–985.

[9] Y. A. I. Mohamed, "Mitigation of dynamic, unbalanced, and harmonic voltage disturbances using grid-connected inverters with LCL filter," *IEEE Trans. Ind. Electron.*, vol. 58, no. 9, pp. 3914–3924, Sep. 2011.

[10] S. Weckx, C. Gonzalez, and J. Driesen, "Reducing grid losses and voltage unbalance with PV inverters," in *Proc. IEEE PES General Meeting Conf. Expo.*, Jul. 2014, pp. 1–5.

[11] O. Bassey and K. L. Butler-Purry, "Modeling single-phase PQ inverter for unbalanced power dispatch in islanded microgrid," in *Proc. IEEE Texas Power Energy Conf.*, Feb. 2019, pp. 1–6.

[12] X. Quan, X. Dou, Z. Wu, M. Hu, H. Song, and A. Q. Huang, "A novel dominant dynamic elimination control for voltage-controlled inverter," *IEEE Trans. Ind. Electron.*, vol. 65, no. 8, pp. 6800–6812, Aug. 2018.

[13] X. Fu and S. Li, "Control of single-phase grid-connected converters with LCL filters using recurrent neural network and conventional control methods," *IEEE Trans. Power Electron.*, vol. 31, no. 7, pp. 5354–5364, Jul. 2016.

[14] M. Ciobotaru, R. Teodorescu, and F. Blaabjerg, "Control of single-stage single-phase PV inverter," *EPE J.*, vol. 16, no. 3, pp. 20–26, 2006.

[15] M. Ebrahimi, S. A. Khajehoddin, and M. Karimi-Ghartemani, "Fast and robust single-phase *dq* current controller for smart inverter applications," *IEEE Trans. Power Electron.*, vol. 31, no. 5, pp. 3968–3976, May 2016.

[16] S. Dasgupta, S. K. Sahoo, and S. K. Panda, "Single-phase inverter control techniques for interfacing renewable energy sources with microgrid—Part I: Parallel-connected inverter topology with active and reactive power flow control along with grid current shaping," *IEEE Trans. Power Electron.*, vol. 26, no. 3, pp. 717–731, Mar. 2011.

[17] A. M. Bouzid, J. M. Guerrero, A. Cheriti, M. Bouhamida, P. Sicard, and M. Benghanem, "A survey on control of electric power distributed generation systems for microgrid applications," *Renewable Sustain. Energy Rev.*, vol. 44, no. C, pp. 751–766, 2015.

[18] P. Chiang Loh, M. J. Newman, D. N. Zmood, and D. G. Holmes, "A comparative analysis of multiloop voltage regulation strategies for single and three-phase ups systems," *IEEE Trans. Power Electron.*, vol. 18, no. 5, pp. 1176–1185, Sep. 2003.

[19] K. Xie, G. Hu, H. Yi, Z. Lyu, and Y. Xiang, "A novel digital control method of a single-phase grid-connected inverter based on a virtual closed-loop circuit and complex vector representation," *Energies*, vol. 10, no. 12, 2017, Art. no. 2068.
[20] P. Verdelho and G. D. Marques, "DC voltage control and stability analysis of PWM-voltage-type reversible rectifiers," *IEEE Trans. Ind. Electron.*, vol. 45, no. 2, pp. 263–273, Apr. 1998.
[21] J. Shen, S. Schröder, H. Stagge, and R. W. De Doncker, "Precise modeling and analysis of dq-frame current controller for high power converters with low pulse ratio," in *Proc. IEEE Energy Convers. Congr. Expo.*, 2012, pp. 61–68.
[22] J.-S. Yim, S.-K. Sul, B.-H. Bae, N. R. Patel, and S. Hiti, "Modified current control schemes for high-performance permanent-magnet ac drives with low sampling to operating frequency ratio," *IEEE Trans. Ind. Appl.*, vol. 45, no. 2, pp. 763–771, Mar./Apr. 2009.
[23] J. Shi, J. Shen, B. Qu, H. She, and Z. Tan, "High-performance complex controller for high-power converters with low pulse ratios," in *Proc. 9th Int. Conf. Power Electron. ECCE Asia*, 2015, pp. 2180–2187.
[24] J. Holtz, J. Quan, J. Pontt, J. Rodríguez, P. Newman, and H. Miranda, "Design of fast and robust current regulators for high-power drives based on complex state variables," *IEEE Trans. Ind. Appl.*, vol. 40, no. 5, pp. 1388–1397, Sep./Oct. 2004.
[25] R. Bhattarai, N. Gurung, and S. Kamalasadan, "Minimum variance controller based adaptive control for doubly fed induction generator," in *Proc. North Amer. Power Symp.*, Sep. 2016, pp. 1–6.
[26] N. Gurung, R. Bhattarai, and S. Kamalasadan, "Control of grid connected inverters using minimum variance adaptive architecture," in *Proc. IEEE Int. Conf. Power Electron., Drives Energy Syst.*, Dec. 2016, pp. 1–6.
[27] R. Bisht, S. Subramaniam, R. Bhattarai, and S. Kamalasadan, "Adaptive minimum variance control of grid connected single phase inverters in synchronously rotating *dq* reference frame," in *Proc. IEEE Ind. Appl. Soc. Annu. Meeting*, Sep. 2018, pp. 1–10.
[28] R. Zhang, M. Cardinal, P. Szczesny, and M. Dame, "A grid simulator with control of single-phase power converters in d-q rotating frame," in *Proc. IEEE 33rd Annu. IEEE Power Electron. Specialists Conf. Proc.*, 2002, vol. 3, pp. 1431–1436.
[29] R. Bisht, S. Subramaniam, R. Bhattarai, and S. Kamalasadan, "Active and reactive power control of single phase inverter with seamless transfer between grid-connected and islanded mode," in *Proc. IEEE Power Energy Conf. Illinois*, Feb. 2018, pp. 1–8.
[30] S. Golestan and J. M. Guerrero, "Conventional synchronous reference frame phase-locked loop is an adaptive complex filter," *IEEE Trans. Ind. Electron.*, vol. 62, no. 3, pp. 1679–1682, Mar. 2015.
[31] K. Ogata, *Modern Control Engineering*, 4th ed. Upper Saddle River, NJ, USA: Prentice-Hall, 2001.
[32] W. H. Kersting, "Radial distribution test feeders," in *Proc. IEEE Power Eng. Soc. Winter Meeting. Conf. Proc.*, Jan. 2001, vol. 2, pp. 908–912.
[33] R. Teodorescu, F. Blaabjerg, M. Liserre, and P. C. Loh, "Proportional-resonant controllers and filters for grid-connected voltage-source converters," *IEE Proc. - Elect. Power Appl.*, vol. 153, no. 5, pp. 750–762, Sep. 2006.

Robin Bisht (Student Member, IEEE) received the B.Tech. degree in electrical and electronics engineering from the Visvesvaraya National Institute of Technology, Nagpur, India, in 2013, and the M.Sc. degree in electrical and computer engineering from the University of North Carolina, Charlotte, NC, USA, in 2016, where he is currently working toward the Ph.D. degree in electrical engineering.

His research interests include microgrids, smart inverters, application of power electronics in power systems, and control of power system.

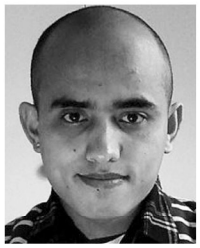

Rojan Bhattarai (Member, IEEE) received the B.E. degree in electrical engineering from the Institute of Engineering, Pulchowk Campus, Tribhuvan University, Kirtipur, Nepal, in 2012, and the Ph.D. degree in electrical engineering from the University of North Carolina at Charlotte, Charlotte, NC, USA, in Fall 2014.

He is currently a Power System Research Engineer with Idaho National Laboratory, Idaho Falls, ID, USA. Previously, he was a Postdoctoral Research Appointee with Argonne National Laboratory until the end of February, 2020. His current research interests include distributed energy systems integration, modeling and control, stability studies of renewable energy resources integrated bulk power grid and use of distributed energy resources for supporting stability of power grid, and doubly fed induction generator (DFIG) based wind generation systems.

Shashank Subramaniam (Member, IEEE) received the B.Tech. degree in electrical and electronics engineering from the National Institute of Technology, Tiruchirappalli, India, in 2016, and the M.Sc. degree in electrical and computer engineering from the University of North Carolina, Charlotte, NC, USA, in 2018.

He is currently an Associate Automation Engineer with Schweitzer Engineering Laboratories, Charlotte, NC, USA.

Sukumar Kamalasadan (Senior Member, IEEE) received the B.Tech. degree in electrical and electronics engineering from the University of Calicut, Malappuram, India, in 1991, the M.Eng. degree in electrical power systems management from the Asian Institute of Technology, Bangkok, Thailand, in 1999, and the Ph.D. degree in electrical engineering from the University of Toledo, Toledo, OH, USA, in 2004.

He is currently a Professor with the Department of Electrical and Computer Engineering, University of North Carolina at Charlotte, Charlotte, NC, USA. His research interests include intelligent and autonomous control, power systems dynamics, stability and control, smart grid, microgrid, and real-time optimization, and control of power system.

Dr. Kamalasadan has won several awards including the NSF CAREER Award and the IEEE Best Paper Award.